Supplementary Materials for

Degradation of Methylammonium Lead Iodide Perovskite Structures through Light and Electron Beam Driven Ion Migration

Authors:

Haifeng Yuan[1,*], Elke Debroye[1], Kris Janssen[1], Hiroyuki Naiki[1], Christian Steuwe[2], Gang Lu[1], Michèle Moris[1], Emanuele Orgiu[4], Hiroshi Uji-i[1, 3], Frans De Schryver[1], Paolo Samorì[4], Johan Hofkens[1, 5] * and Maarten Roeffaers[2, *]

Affiliations:

[1] Department of Chemistry, KU Leuven, Celestijnenlaan 200F, B-3001 Leuven, Belgium.

[2] Department of Microbial and Molecular Systems, Centre for Surface Chemistry and Catalysis, KU Leuven, B-3001 Leuven, Belgium.

[3] Research Institute for Electronic Science, Hokkaido University, N20W10, Kita-Ward, 001-0020 Sapporo, Japan.

[4] ISIS & icFRC, Université de Strasbourg & CNRS, 8 allée Gaspard Monge, 67000 Strasbourg, France

[5] Nano-Science Center, University of Copenhagen, Universitetsparken 5, 2100 Copenhagen, Denmark.

*To address correspondence:

haifeng.yuan@chem.kuleuven.be;

maarten.roeffaers@biw.kuleuven.be;

johan.hofkens@chem.kuleuven.be.

1. $CH_3NH_3PbI_3$ synthesis.

1.1 Materials. All the chemicals were used as received, including lead (II) iodide (99%, Sigma-Aldrich), hydriodic acid (57 wt% in water, Aldrich), methylamine (33 wt% in absolute ethanol, Sigma-Aldrich), γ-butyrolactone, diethyl ether, ethanol for spectroscopy, absolute ethanol, and toluene.

1.2 Preparation of methylammonium iodide (CH_3NH_3I). Methylammonium iodide was synthesized by a typical procedure [1]. 27.8 mL of methylamine and 30 mL of hydriodic acid are reacted in a 150 mL round-bottom flask at 0 °C for 2 hours with stirring. The precipitate was recovered by using a rotary evaporator through removing solvents at 50 °C. The as-obtained product was re-dissolved in 80 mL of ethanol, re-crystallized by the addition of 300 mL of diethyl ether twice and finally washed by absolute ethanol once. The pure methylammonium iodide was collected and dried at 60 °C in a vacuum oven for 24 hours.

1.3 Perovskite films [1]**.** 0.395 g methylammonium iodide and 1.175 g lead (II) iodide were dissolved into 2 mL γ-butyrolactone at 60 ºC while stirring overnight. Perovskite film sample was prepared by spin-coating the 60 ºC solution onto an ITO-coated coverglass with a speed of 1500 rpm for 60 seconds. Right after spin-coating, the sample was heated at 90 ºC for 20 minutes. The sample was then subjected to optical and SEM measurements.

1.4 Perovskite crystals [2]**.** 92 mg of lead (II) iodide and 32 mg of methylammonium iodide were mixed in 2 mL of γ-butyrolactone and stirred at 60 ºC overnight to completely dissolve the compounds. 0.4 mL of the mixture was injected into 15 mL of toluene while stirring. The suspension was left still overnight and was then washed by

replacing the supernatant with toluene twice. The perovskite nanocrystal was obtained after spin-coating the suspension onto a coverslip or an ITO coverslip at 1500 RPM for 60 seconds.

1.5 PbI_2 nanoplates. 175 mg of lead (II) iodide was added to 10 mL water and was stirred at 70 ºC for an hour to get a saturated solution. After leaving it still at 70 ºC for 10 minutes, the clear colorless supernatant liquid was taken and sonicated in a 20 ºC water bath for 5 minutes, leading to the formation of lead (II) iodide crystals. The yellowish suspension was then spin-coated onto an ITO-coated glass slide with a speed of 1500 rpm for 60 seconds.

2. Instruments.

2.1 Integrated optical and electron microscope.

The integrated luminescence and electron microscope (ILEM) system consists of a FEI Quanta FEG-250 environmental scanning electron microscope (SEM), equipped with a modified door assembly provided by Delmic BV, The Netherlands [3]. This door features an optically transparent window which enables the transmission of excitation and emission light and holds both an EM-CCD camera (Image-EM X2, Hamamatsu) and optomechanics. Additionally, the original SEM stage is replaced by one that is capable of holding a high numerical aperture oil-immersion objective lens (Plan Apo VC 100X, NA 1.4, Nikon) which enables high-resolution imaging in combination with vacuum compatible immersion oil. The ILEM instrument is further equipped with a laser illumination system featuring 6 distinct sources (405 nm, 445 nm, 488 nm, 532 nm, 561 nm and 642 nm, LightHub, Omicron). The 532 nm output is employed as the

excitation source in this study. A compact spectrometer (USB4000, OceanOptics) is used for the spectral measurements in the ILEM instrument.

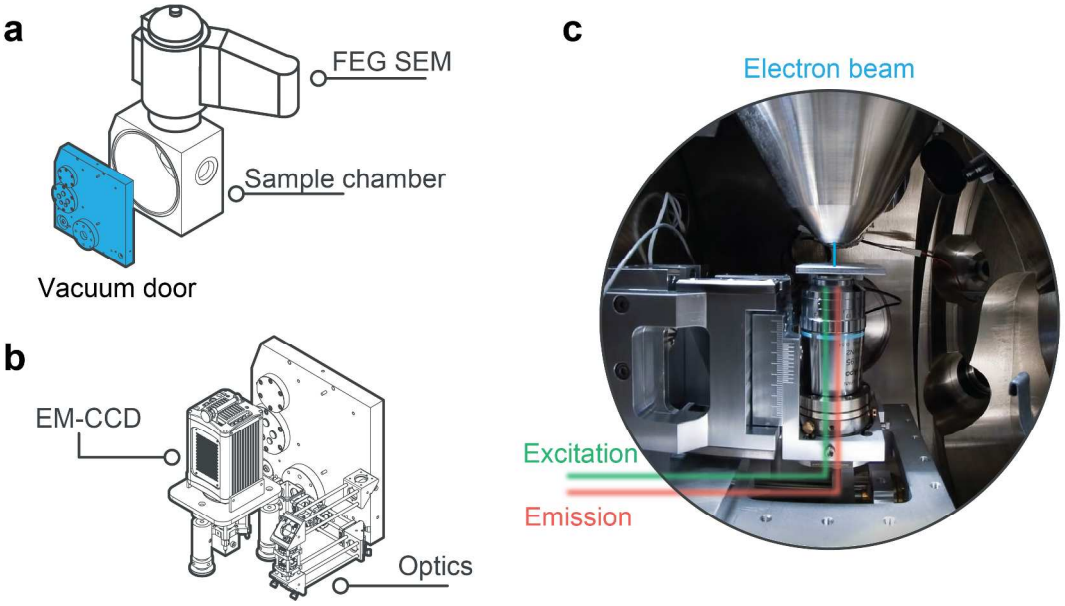

Fig. S1. Schematic drawing of the iLEM setup. (a) The modified chamber door on the FEI FEG-250 SEM instrument. (b) Optics and EM-CCD are mounted on the extension part of the modified SEM chamber door. (c) The view inside the modified sample chamber, where the optical beam and the electron beam are overlaid to each other.

2.2 Confocal optical microscope.

The confocal microscopy results were obtained on an inverted optical microscope (TiU, Nikon) equipped with a scanning stage (Combiscope-1000, AIST-NT). The diffraction-limited focused light excitation was provided by a continuous wave 532 nm laser (Cobolt AB). Circular polarization at the sample was achieved by tuning half-wavelength (lambda/2) and quarter-wavelength (lambda/4) wave plates. The spectra were collected by a spectrometer (iHR-320, Horiba) equipped with a cooled electron multiplying charge-

coupled device (CCD) camera (Newton-920, Andor). An air objective with a NA of 0.9 was used for spectral measurements.

2.3 Atomic force microscopy (AFM).

Smart-1000 AFM (AIST-NT) was used for AFM measurements under ambient conditions in tapping mode with a Si tip (cantilever length, 140 μm; resonant frequency, 200-400 kHz; spring constant, 25-95 N/m) at a scanning rate of 0.5 Hz and sample line of 1024.

2.4 X-ray diffraction (XRD)

XRD measurements on the prepared perovskite materials were carried out on a STOE STADI P COMBI instrument equipped with an imaging plate (IP position sensitive detector) as the detector. The diffraction was measured using Cu Kα1 radiation in transmission mode with a focusing Ge (111) monochromator.

3. Supporting results

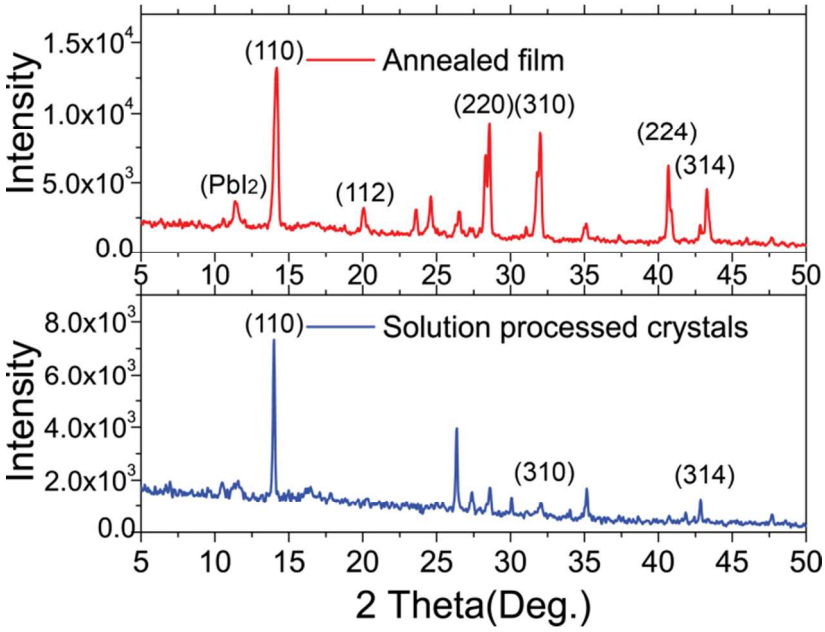

Fig. S2. XRD patterns of perovskite samples prepared using different methods. The observed patterns match those reported in literature [4].

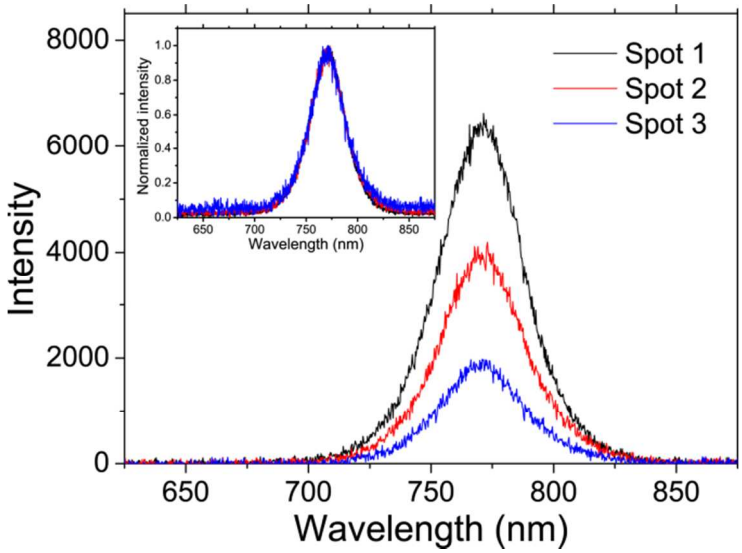

Fig. S3. Photoluminescence spectra acquired at different positions on the perovskite films. Though the emission intensities are different, they show almost identical emission spectra.

The peak centre locates at 768 nm. The inset shows that the normalized spectra overlay with each other.

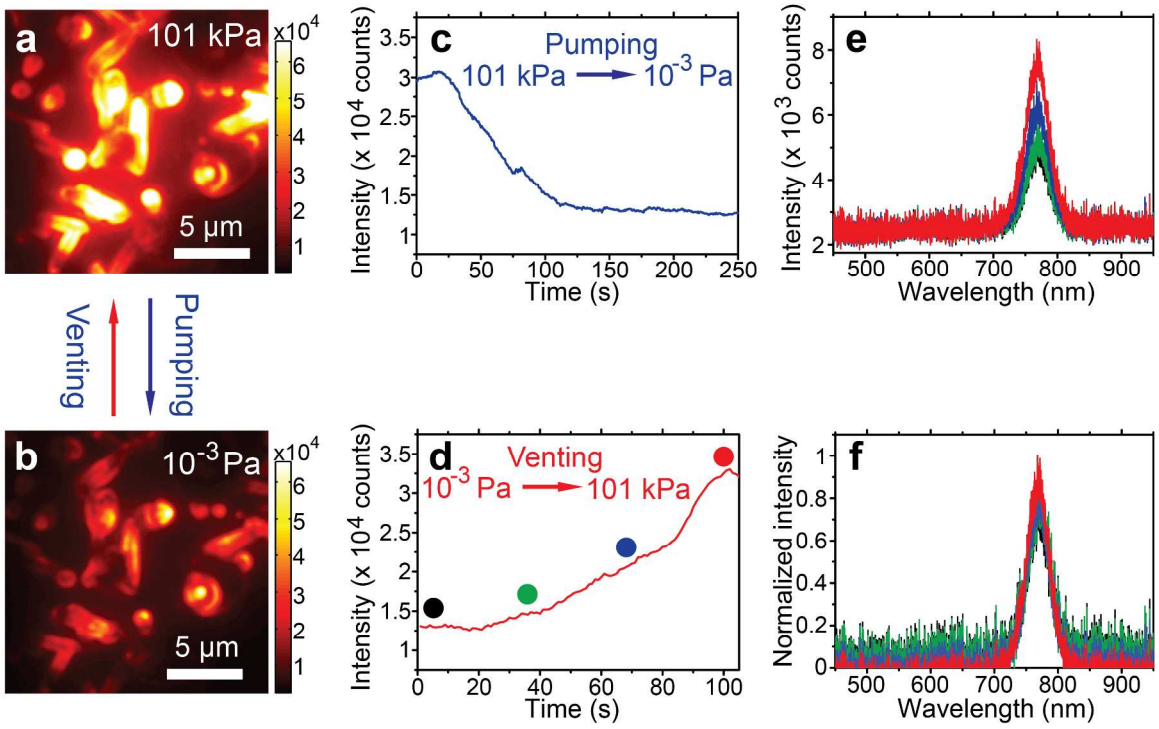

Fig. S4. Perovskite structures show different photoluminescence intensities in different environments under identical excitation. (a) Photoluminescence image taken at ambient conditions. (b) Photoluminescence image on the same perovskite crystal under high vacuum. (c) Photoluminescence time trace during pumping the sample chamber from ambient pressure to high vacuum. (d) Photoluminescence intensity time trace during venting the sample chamber from high vacuum to the ambient pressure. (e) Emission spectra at different stages of chamber venting. The coloured curves correspond to the time highlighted with the coloured dots in D. (f) Normalized emission spectra show no

spectral shifts during the environment changes between ambient conditions and high vacuum.

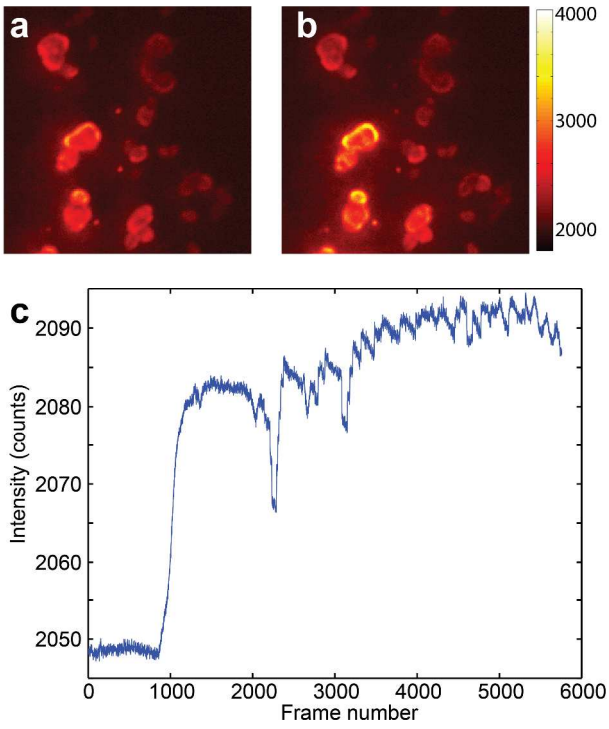

Fig. S5. Changes in optical collection efficiencies at ambient condition and at high vacuum. (a) and (b) Photoluminescence images of the same nanodiamonds under high vacuum and under ambient conditions, respectively. The color bar represents the luminescence intensity in each image frame. (c) Photoluminescence intensity time trace during venting the SEM sample chamber. The background level is 1940 counts. The changes in collection efficiency due to high vacuum are about 28%. Calculated with (2090-2048)/(2090-1940) = 28%. The sudden drops in intensity come from mechanical drifts of the sample stage during pumping of the SEM chamber.

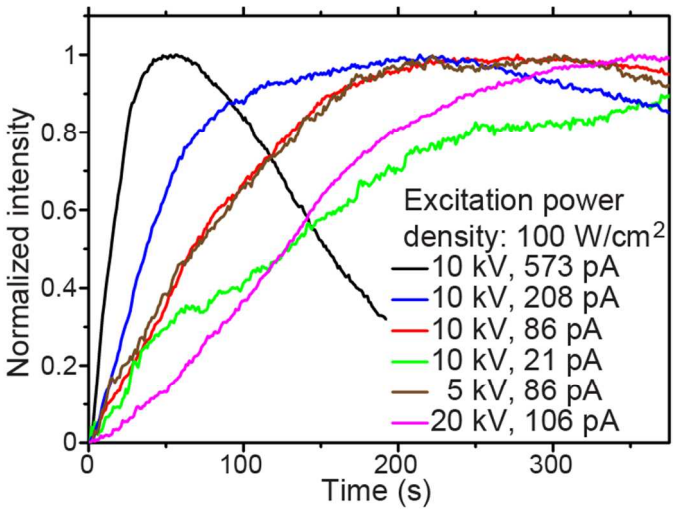

Fig. S6. Rates of photoluminescence recovery strongly depend on the electric current. To compare the influence of current density on the rate of photoluminescence recovery, different currents (21 pA, 86 pA, 106 pA, 208 pA and 573 pA) and acceleration voltages are applied. A low laser power density of 100 W/cm^2 is used. Photoluminescence time traces are normalized by their minima and maxima in intensities. The minimum intensities in the time traces are brought to time 0 to compare them. Under the same acceleration voltage of 10 kV, the stronger beam current leads to a faster recovery in photoluminescence. Under the same beam current of 86 pA, different acceleration voltages of 5 kV and 10 kV show identical photoluminescence recovery rates. However, the photoluminescence recovery becomes much slower when the acceleration voltage is raised to 20 kV, likely due to material destruction by high energy electrons.[2]

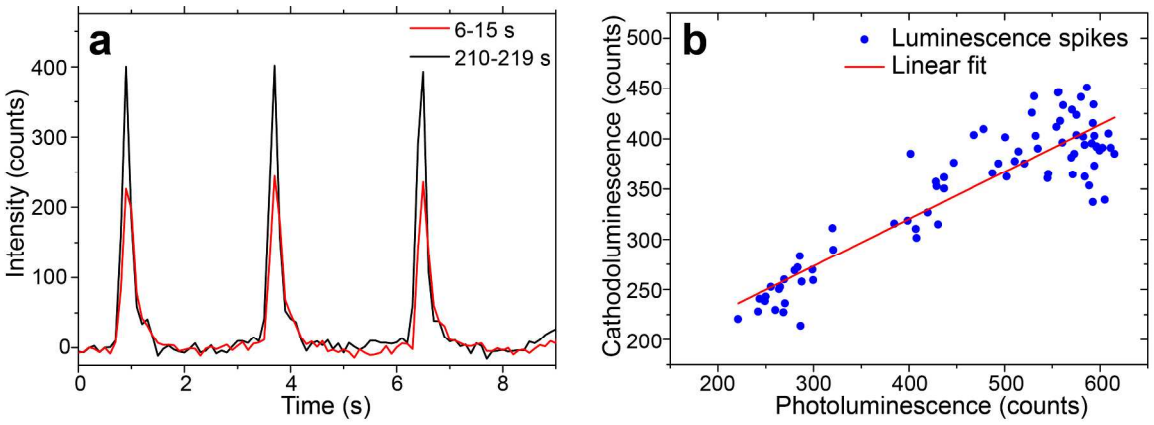

Fig. S7. Enhanced electron-induced luminescence under prolonged e-beam scanning in Fig. 1d. **(a)** Two fragments of the trace shown in Fig. 1d, respectively 6-15 s and 210-219 s, are compared by subtracting the photoluminescence as baselines. The average intensity of the electron-induced luminescence increased by two fold from 200 counts to 400 counts. Alongside with the recovery of photoluminescence, the electron-induced luminescence also increases by a factor of 2. (b) The enhanced cathodoluminescence linearly correlate with the recovering photoluminescence.

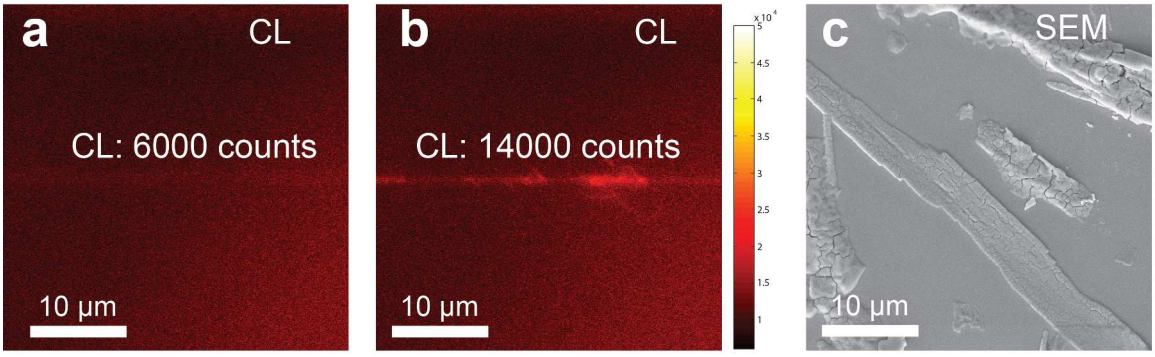

Fig. S8. Enhanced cathodoluminescence by continuous e-beam scanning. (a) Cathodoluminescence image during one line scanning with the e-beam on the freshly prepared perovskite structure. The e-beam current is 86 pA. The acceleration voltage is

10 kV. The cathodoluminescence intensity after subtracting the background is approximately 6000 counts. (b) Cathodoluminescence image during one line scanning with the e-beam after continuous e-beam scanning for 5 minutes. The cathodoluminescence intensity at the same position after subtracting the background increased to 14000 counts. The same color scale, representing the luminescence intensity in each image frame, applies to A and B. (c) SEM micrograph of the same sample area after the experiment. Cathodoluminescence changes can be observed in the perovskite film under the scanning e-beam. The cathodoluminescence is weak in freshly-made perovskite films but increases under continuous e-beam scanning by a factor of 2, resembling the enhancement factor found in the electron-induced luminescence spikes in Fig. S7. Therefore, the luminescence spikes observed here are most likely due to cathodoluminescence.

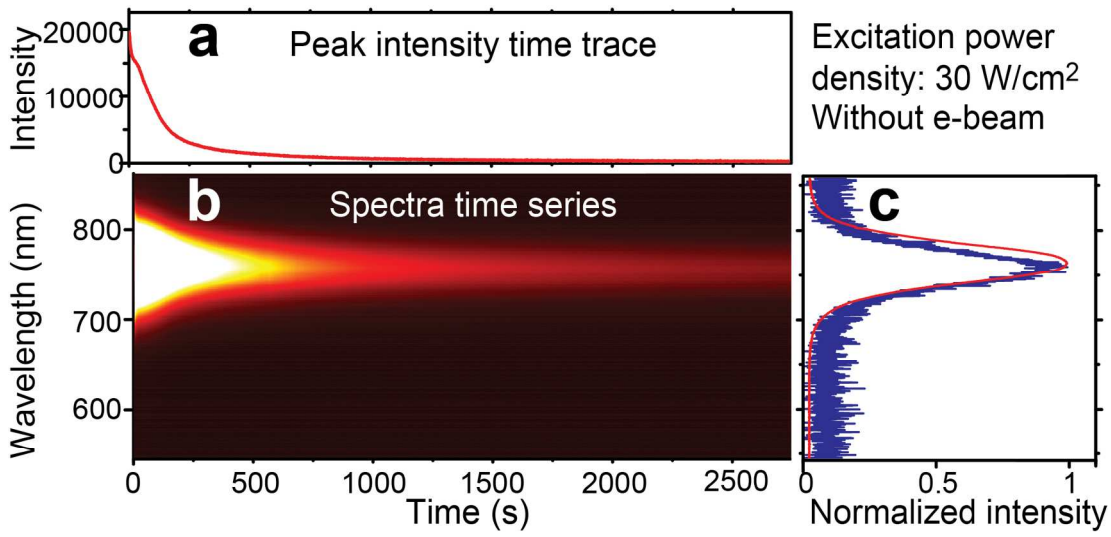

Fig. S9. Photoluminescence spectra time series during light driven degradation in the perovskite structure. (a-b) Photoluminescence intensity time trace and the corresponding spectral evolution under laser illumination (30 W/cm^2). (c) Normalized emission spectra

taken at the beginning and at the end of the series, in red (centred at 770 nm) and in blue (centred at 766 nm) respectively.

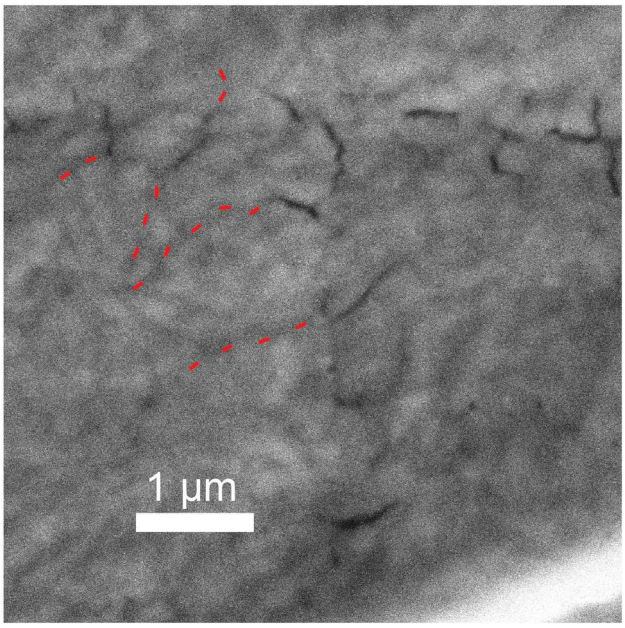

Fig. S10. Enlarged SEM micrograph on the "T" pattern drawn with the e-beam. Grain boundaries can be recognized. Several dashed red lines, serving as guides to eye, highlight the original grain boundaries in the perovskite structure. The deep cracks induced by the e-beam are along the grain boundaries.

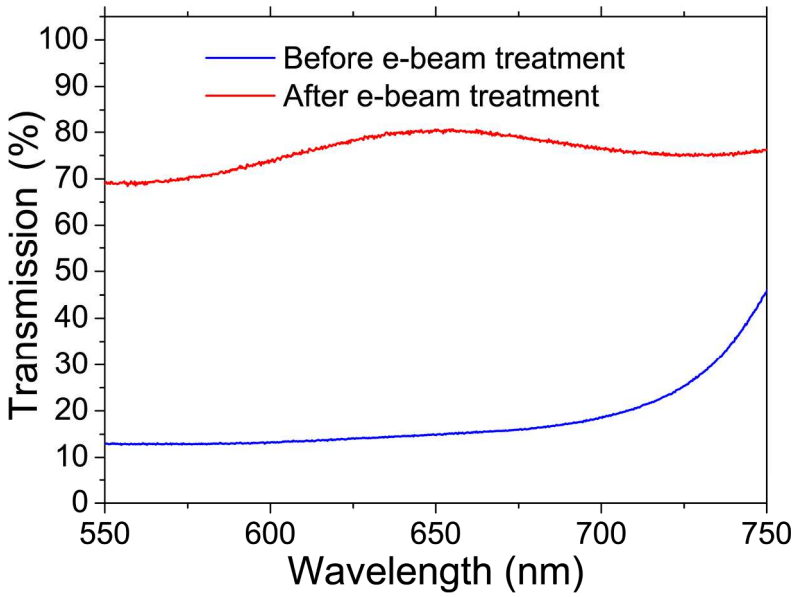

Fig. S11. Transmission spectra acquired on the perovskite film before (in blue color) and after (in red colour) electrical degradation. The transmission rate at 500 nm is increased from 13% to 70%, indicating reduced light absorption by the structure after electrical degradation.

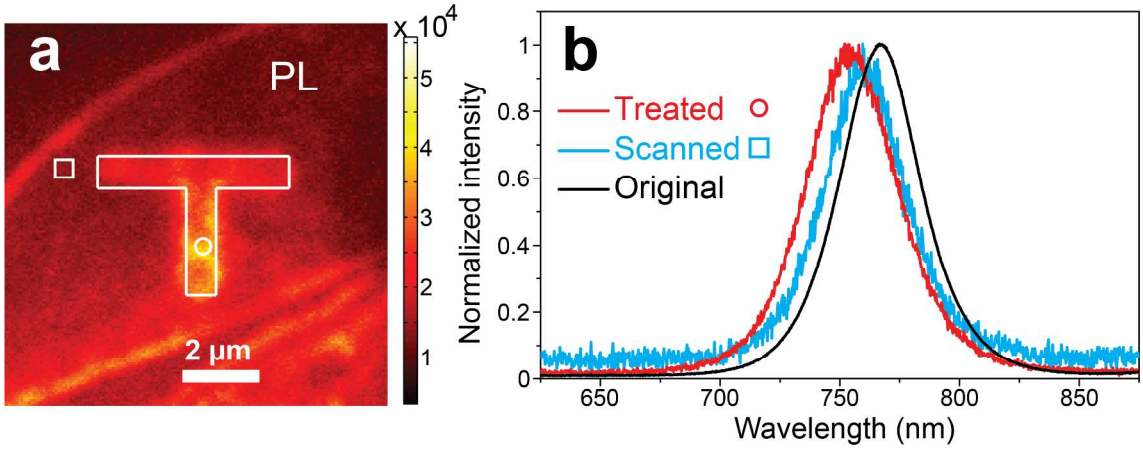

Fig. S12. Spectral shifts are observed in the electrically degraded regions in Fig. 2. (a) Photoluminescence image of the sample region shown in Fig. 2a-d. (b) Photoluminescence spectra measured before and after the e-beam treatment. After

drawing the “T” pattern with the e-beam, the photoluminescence spectrum blue-shifts from 767 nm to 755 nm. The remaining part which is only subjected to the scanning e-beam during SEM image acquisition also shows a spectral shift from 767 nm to 761 nm.

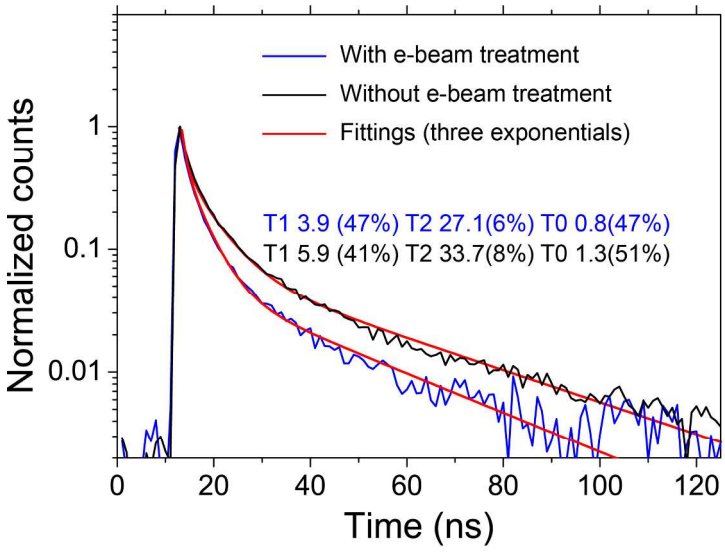

Fig. S13. Photoluminescence decay times measured on perovskite film areas with (in blue colour) and without (in black colour) e-beam treatment. The decay curves were fit with a three exponential function. The shortest characteristic time (T0) is likely from the instrumental response function. For the untreated film, the characteristic times are 5.9 ns and 33.7 ns. For the film area treated with the e-beam, the characteristic times shorten to 3.9 ns and 27.1 ns respectively.

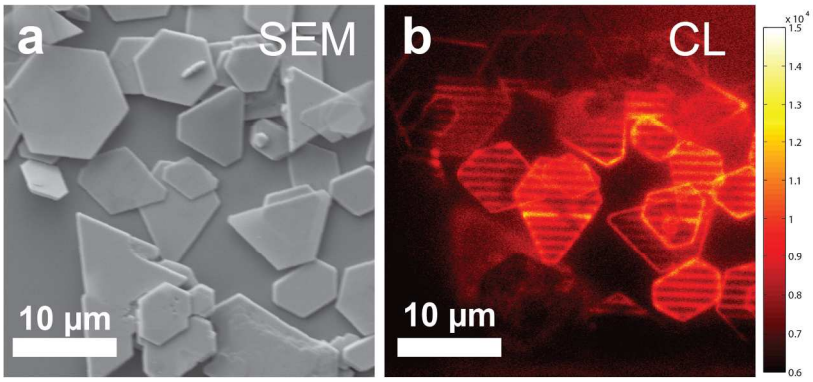

Fig. S14. Cathodoluminescence of PbI_2 nanoplates. (a) SEM image on PbI_2 nanoplates. The thickness is approximately 100 nm ~ 200 nm. (b) Cathodoluminescence image on the same sample area. The e-beam parameters and EMCCD parameters are the same to those used in figure S7.

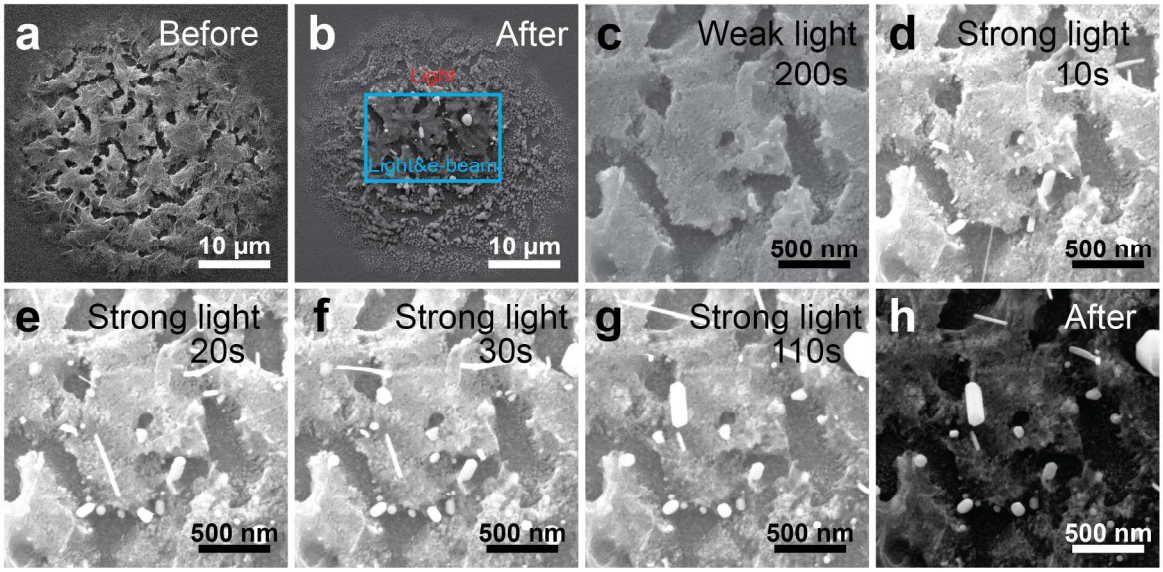

Fig. S15. Structural evolution of a thick perovskite film during a simultaneous SEM and optical measurement. (a) SEM image before the measurement. (b) SEM image after the simultaneous SEM and optical measurement. The e-beam was scanned in the centre area of the sample highlighted with the solid cyan square. The laser beam covered the entire

field of view. (c) SEM image acquired after 200 seconds of light illumination of 1.4 kW/cm^2. (d-g) SEM images acquired at 10 seconds, 20 seconds, 30 seconds and 110 seconds after increasing the light power density to 12 kW/cm^2. At elevated light intensity, nanoparticles started to form, to grow and to vanish kinetically. (h) SEM image taken after the experiment. The morphology becomes static under SEM, indicating the strong role of light in crystal formation and in inducing changes at the perovskite surface.

Movie S1. Drawing the "T" pattern using the e-beam. The field of view is about 15 μm.

Movie S2. Interplay of electrical and photo- degradation under weak and strong light illuminations.

Movie S3. Degradation of two clusters of perovskite cuboids under simultaneous optical and electron microscopy.

References and Notes:

[1] Y. Tian, A. Merdasa, M. Peter, M. Abdellah, K. Zheng, C. S. Ponseca, T. Pullerits, A. Yartsev, V. Sundström, I. G. Scheblykin, *Nano Lett.* 2015, 15, 1603.
[2] F. Zhu, L. Men, Y. Guo, Q. Zhu, U. Bhattacharjee, P. M. Goodwin, J. W. Petrich, E. A. Smith, J. Vela, *ACS Nano* 2015, 9, 2948.
[3] N. Liv, A. C. Zonnevylle, A. C. Narvaez, A. P. J. Effting, P. W. Voorneveld, M. S. Lucas, J. C. Hardwick, R. A. Wepf, P. Kruit, J. P. Hoogenboom, *PLoS ONE* 2013, 8, e55707.
[4] T. Baikie, Y. Fang, J. M. Kadro, M. Schreyer, F. Wei, S. G. Mhaisalkar, M. Graetzel, T. J. White, *J. Mater. Chem. A* 2013, 1, 5628.